Available online at www.sciencedirect.com
ScienceDirect
Optics Communications 273 (2007) 99–104
OPTICS COMMUNICATIONS
www.elsevier.com/locate/optcom

Transmission properties and band structure of a segmented dielectric waveguide for the terahertz range

H. Němec [a], P. Kužel [a,*], J.-L. Coutaz [b], J. Čtyroký [c]

[a] Institute of Physics, Academy of Sciences of the Czech Republic, Na Slovance 2, 182 21 Prague 8, Czech Republic
[b] Laboratoire d'Hyperfréquences et Caractérisation, Université de Savoie, 73376 Le Bourget du Lac Cedex, France
[c] Institute of Photonics and Electronics, Academy of Sciences of the Czech Republic, Chaberská 57, 182 51 Prague 8, Czech Republic

Received 10 October 2006; received in revised form 7 December 2006; accepted 8 December 2006

Abstract

In this paper we investigate the band structure of guided modes in a segmented planar waveguide for the terahertz range. The dispersion curves are obtained using two different methods. The first approach is based on a close relationship between the band structure and narrow resonances in transmission spectra: transmission spectra are therefore calculated using a transfer matrix method and compared to the experimental ones. The second technique involves a modal analysis approach of diffraction gratings and it is used for direct calculation of the band structure. Propagation of THz guided waves along the grating considered as a segmented dielectric waveguide is also investigated using a bi-directional mode expansion and propagation method. All approaches are compared to each other and discussed.

1. Introduction

Waveguiding structures with in-plane periodic pattern show very rich dispersion features: this is true namely for the probing frequencies for which the Bragg diffraction condition is close to be satisfied. The usefulness of such structures has already been demonstrated in integrated optics namely as stop-band filters, Bragg mirrors, input and output couplers and signal multiplexers [1–3] or in nonlinear optics for achieving quasi-phase-matching condition for second harmonic generation [4,5]. The most remarkable dispersion properties are observed in the cases when the dielectric constant along the waveguide direction exhibits a large contrast of periodic modulation. This occurs e.g., in deep waveguide gratings or in segmented waveguides, which consist of rectangular stripes of high index material separated by air or embedded in a low-index host material. Such structures have been extensively studied, mostly in the optical domain: starting by pioneering works of Nevière [6] and Peng [7] on grating couplers and periodic waveguides, theoretical studies were subsequently performed on shallow gratings or gratings with weak permittivity modulation [8], on deeply etched waveguide gratings [9], on infinitely thick gratings [10,11], or on general segmented gratings [12,13] where, however, only narrow frequency range has been usually considered. More recently, based on a modal analysis, smart filtering properties of such segmented waveguides have been proposed and demonstrated in the THz range [14,15]. The analysis of the band structure of these modulated waveguides is important, among others, for understanding out-of-plane radiation losses of two-dimensional photonic crystals in dielectric membranes and planar waveguides [16,17].

This paper focuses on the terahertz (THz) spectral range (1 THz corresponds to a wavelength of 300 μm). This part of the electromagnetic spectrum became recently very easily accessible using the so called opto-electronic approach [18]. The technique enables fast, broadband and phase-sensitive measurements of transmission and/or reflection spectra of various materials and structures, e.g., characterization of the electromagnetic response of mock-ups with much larger

* Corresponding author. Tel.: +420 266 052 176; fax: +420 286 890 527.
E-mail address: kuzelp@fzu.cz (P. Kužel).

0030-4018/$ - see front matter © 2006 Elsevier B.V. All rights reserved.
doi:10.1016/j.optcom.2006.12.016

or smaller sizes than those used in optical or radio-frequency devices [19]. Indeed, the THz range is of particular interest regarding the design, characterization and application of photonic bandgap structures: the appropriate structures have submillimeter lattice period and their fabrication by mechanical micromachining [20] or photolithography and ion etching [21] is easier than that of actual micrometer or sub-micrometer sized optical devices. At the same time, due to the applicability of the scaling laws [22], the important conclusions of both theoretical and experimental investigations in the THz range can be extended both to optical and radio-frequency regions (taking properly the dispersion properties of materials into account).

Recently, THz data have been published for a segmented silicon grating structure exhibiting a large number of both sharp and broad spectral features [19]. In the current paper, we provide an interpretation of these measurements. In order to explain the experimental data we first apply a transfer matrix method [23] to calculate the transmittance spectra of the structure. Based on these spectra, the reconstruction of the band structure of guided and leaky modes is tentatively performed. Next, we apply a rigorous modal approach [7] as a tool for the direct calculation of the band structure. Both kinds of theoretical results are compared with each other and with experiments and discussed.

2. Description of models

The investigated structure is shown in Fig. 1. Following Ref. [19] we assume in our calculations the following geometrical characteristics of the structure: grating thickness $d = 210\ \mu\text{m}$, period $L = 385\ \mu\text{m}$, filling factor (ratio between the integrated areas of silicon and the total grating area) $\xi = 0.455$. The dielectric constant of high-resistivity silicon is $\varepsilon_{\text{Si}} = 11.68$ and its absorption coefficient is small (of the order 1 dB/cm or less at sub-THz frequencies). We assume that the structure is infinite along the y-direction and that the plane of incidence of electromagnetic radiation is perpendicular to the grooves. For this geometry the Maxwell equations split into two independent systems describing separately the TE and TM polarizations.

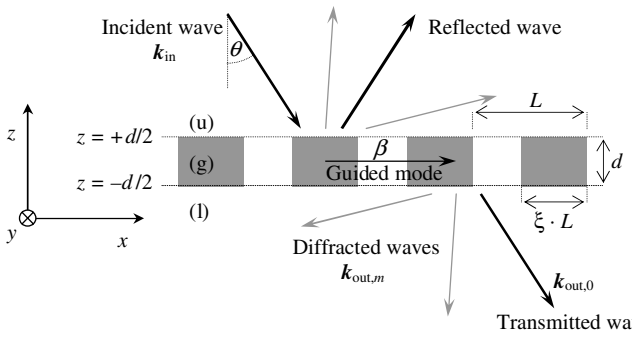

Fig. 1. Scheme of the investigated segmented grating and notation. Dark parts are made of high-resistivity silicon, white parts represent the vacuum. Three regions are defined: upper vacuum space (u), lower vacuum space (l), and grating region (g).

As the experiment in Ref. [19] has been carried out for TE polarization (electric field parallel with the grooves), we restrict the calculations to this case.

Note that models described in Section 2.1 and 2.2 assume an infinite number of grating periods in the x-direction while the numerical calculation presented in Section 2.3 introduces a finite number N of grating segments.

If a grating is illuminated by a plane wave under an angle of incidence θ, a guided mode propagating along the grating may be excited when the wave vector component parallel with the grating surface $k_{\text{in}}^{\parallel}$ is conserved:

$$k_{\text{in}}^{\parallel} \equiv k_0 \sin\theta = \beta + G_m, \tag{1}$$

where $k_0 = \omega/c$ is the wave vector of a plane wave in vacuum, β is the wave vector of the guided mode (restricted to the first Brillouin zone, i.e. $|\beta| < \pi/L$), and $G_m = 2\pi m/L$ is the reciprocal vector of the grating (m is an integer number).

Guided modes can couple into other propagative modes: A part of the energy of the guided mode is carried out of the structure by waves which contribute to the total transmitted, reflected or diffracted field (see Fig. 1). This coupling is at the origin of narrow features in the transmittance or reflectance spectra [24,25].

The frequencies ω_i of these spectral features can be learned from the experimental and/or theoretical transmission spectra for a number of incidence angles θ. Provided the angular dependences $\omega_i(\theta)$ of these features are obtained, a part of the band structure $\omega_i(\beta)$ of the segmented grating can be reconstructed from these results using Eq. (1). The band structure of guided modes describes the Bloch modes which are allowed to travel inside the waveguide along the x-direction with real or complex β. Note that since $|\sin\theta| \leqslant 1$, the transmission or reflections experiments (calculations) provide no information about the modes below the vacuum line, for which $\omega/c < |\beta|$: we call such modes true guided modes since they propagate without radiation loss. The modes characterized by a complex β with non-vanishing imaginary part are referred to as leaky modes [7].

2.1. Transfer matrix method

The transfer matrix method (TMM) for calculation of transmittance and reflectance spectra of two- and three-dimensional periodic structures has been developed and described in detail by Pendry et al. [23,26,27]. In brief, the investigated structure is divided into several planar slices. Transfer matrices then relate the electromagnetic field distributions at the input and output planes of these slices. Matrix elements of the transfer matrix of the entire structure are straightforwardly connected to transmittance, reflectance and diffraction spectra of the entire structure. In these simulations we assumed a small non-vanishing imaginary part of the dielectric constant of the silicon ($\varepsilon = 11.68 + \text{i}0.008$): these losses are introduced to account for absorption especially at higher frequencies.

The calculated complex transmission spectra are compared with the experimental ones in Fig. 2 (the amplitude of the experimental results is taken from Ref. [19]). The agreement between these spectra is very good in the entire frequency range studied. For frequencies below 500 GHz the spectra in Fig. 2 are dominated by wide oscillations. The wavelength of the radiation in this spectral range ($\lambda > 0.6$ mm) exceeds the grating period: in these conditions the structure can be approximately regarded as a homogeneous slab with a dielectric function obeying effective-medium response law. The observed oscillations are then interpreted as a signature of the Fabry–Pérot effect in such a slab. More quantitatively, the effective medium theory defining the refractive index as $n_{\mathrm{eff}} = (\varepsilon_{\mathrm{Si}}\xi + 1 - \xi)^{1/2}$ predicts the lowest Fabry–Pérot maximum at 294 GHz which is to be compared to about 275 GHz deduced from the measured spectra. For frequencies above 300 GHz a series of narrow resonances superposed onto the Fabry–Pérot fringes develops. It is natural to assume that these resonances are caused by excitation of guided modes: this statement will be shown more in details below with the help of the modal approach. Notice that the Rayleigh anomalies corresponding to the passing off of a diffraction order do not produce narrow lines but broader features [28].

In order to draw the band structure of guided waves, the frequencies of the resonances should be determined. We expect that the resonant frequencies can be sufficiently accurately approximated by positions of dips in the transmittance spectra. The band structure obtained from the pointing of the transmittance spectra is shown in Fig. 3: both experimental and theoretical spectra were used and are shown in the plot for the comparison. In the figure we can infer on existence of forbidden bands which usually appear in modulated structures. Note, however, that the shape of the transmittance curves becomes very complicated when modes with similar frequencies simultaneously

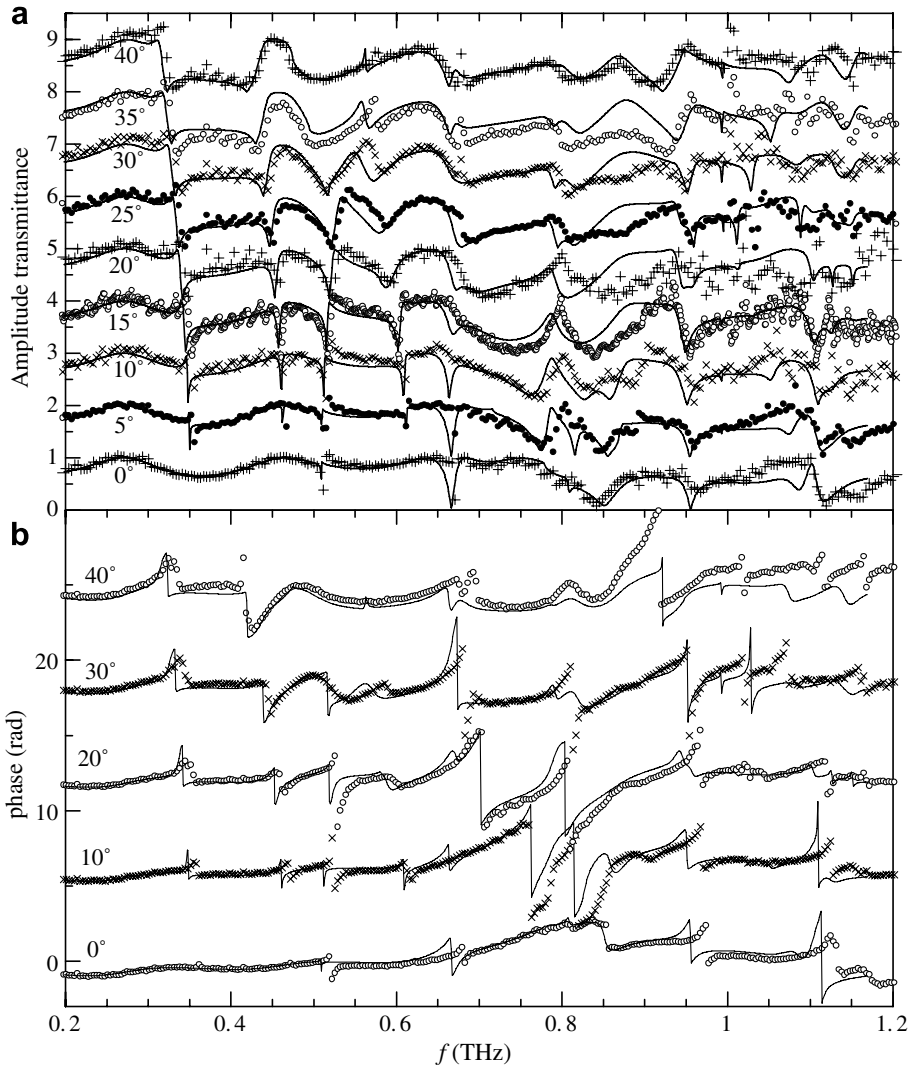

Fig. 2. Transmittance (amplitude and phase) of the segmented grating versus frequency for several angles of incidence. Solid lines: results of the TMM simulation; points: experimental results (from Ref. [19]). For clarity vertical shifts by 1 (amplitude) or 2π (phase) were gradually applied to the data as the angle of incidence is increased.

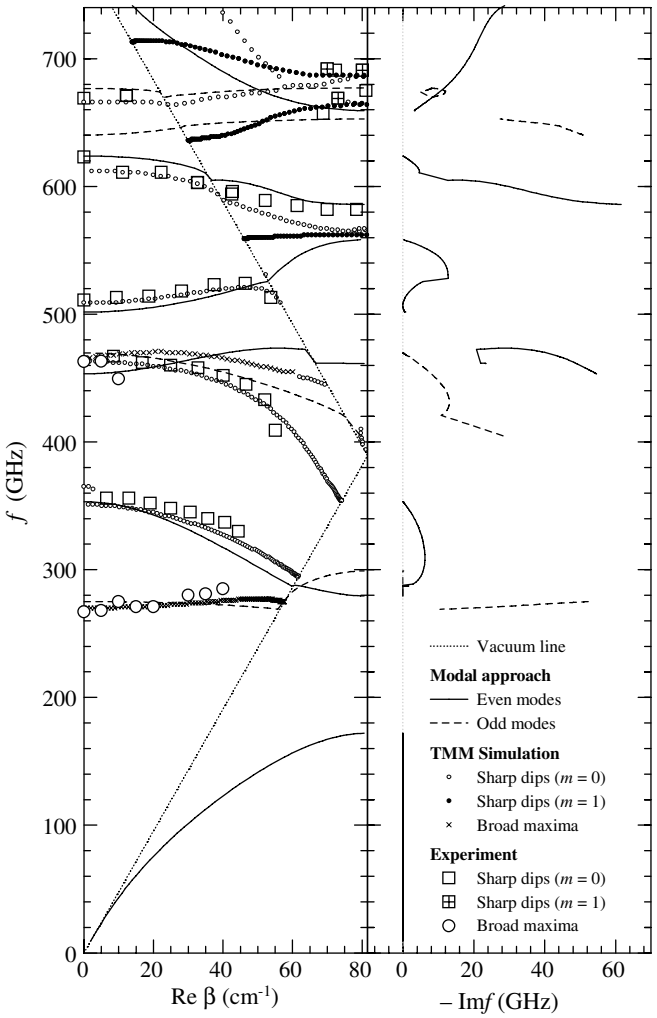

Fig. 3. Band structure of guided and leaky modes in the segmented grating. The plotted data represent a compilation of the results obtained by all the methods discussed. The experimental data were measured in Ref. [19]. The broad maxima are related to transverse Fabry–Pérot resonances of a slab with effective dielectric properties; sharp dips are essentially due to leaky modes. The branches obtained from transmission spectra with $m = 1$ are related to the band folding into the first Brillouin zone [see Eq. (1)].

appear in the spectra: the plot of the band structure one can obtain using this method is then only approximate and not complete.

2.2. Modal method

The electromagnetic theory of gratings called modal approach has been described, e.g. in Refs. [7,12]. The wave equation for the TE polarization ($E_x = E_z = 0$)

$$\frac{\partial^2 E_y}{\partial x^2} + \frac{\partial^2 E_y}{\partial z^2} = -k_0^2 \varepsilon(x,z) E_y \tag{2}$$

is solved. The eigenmodes in the different regions of the space (Fig. 1) can be expanded in terms of the Bloch waves:

$$E_y^{(i)}(x,z) = \sum_{m=-M}^{M} F_m^{(i)} \exp[\mathrm{i}\gamma^{(i)} z + \mathrm{i}(\beta + G_m)x], \tag{3}$$

where the superscript (i) stands for the grating region (g) and for the vacuum regions above and below the grating [(u), (l)] (see Fig. 1). In theory, the sum runs over all reciprocal lattice vectors $G_m (M \to \infty)$. A finite value of the integer M is used in the numerical calculations. Substitution of this sum into (2) yields an eigenvalue problem for the z-components of the wave vector $\gamma^{(i)}$ and eigenvectors $F_m^{(i)}$.

In the vacuum regions the eigenmodes are simple propagative or evanescent plane waves with

$$\gamma_m^{(\mathrm{u,l})} = \sqrt{k_0^2 - (\beta + G_m)^2}, \tag{4}$$

where the sign of the square root is chosen such that $\mathrm{Re}(\gamma_m^{(\mathrm{u,l})}) + \mathrm{Im}(\gamma_m^{(\mathrm{u,l})}) > 0$ [29] which allows for accounting the leaky modes correctly. The eigenmodes in the grating region are superpositions of plane waves with amplitudes $F_{m,q}^{(\mathrm{g})}$ (with $q = -M \ldots M$): these eigenvectors together with corresponding eigenvalues $\gamma_q^{(\mathrm{g})}$ must be found numerically.

The field in each region is expressed as an arbitrary superposition of the eigenmodes (3), e.g. in the region (g) one finds:

$$E_y^{(\mathrm{g})}(x,z) = \sum_{m,q=-M}^{M} F_{m,q}^{(\mathrm{g})} \exp\left[\mathrm{i}\gamma_q^{(\mathrm{g})} z + \mathrm{i}(\beta + G_m)x\right]. \tag{5}$$

The tangential components of the electric and magnetic fields E_y and H_x ($\mathrm{i}\omega\mu_0 H_x = -\partial E_y/\partial z$) must be continuous across the interfaces in the planes $z = \pm d/2$; e.g., $E_y^{(\mathrm{g})}(x, z = d/2) = E_y^{(u)}(x, z = d/2)$ for any x. This leads to a system of linear equations for the amplitudes of the eigenmodes. The zeroes of this system of equations describe guided modes of the segmented waveguide. In this way, it is possible to find for each frequency ω the corresponding set of complex longitudinal propagation constants β. Alternatively, one can look for a set of complex frequencies ω for any real propagation constant β. In this work we use this second possibility. Two kinds of solutions are found: (i) true guided modes for which both β and ω are real and the field outside the grating is evanescent, and (ii) leaky modes for which ω (or β) is complex, i.e., the mode is attenuated when propagating along the structure owing to the radiation of electromagnetic energy out of the structure. In the numerical calculations, the series (3) was limited to the lowest 17 modes ($M = 8$). We have verified that taking $M > 8$ does not improve the numerical results.

2.3. Bi-directional mode expansion and propagation method

In this method, the grating is considered as a segmented waveguide, and wave propagation in both directions *along* the grating is numerically calculated. The grating is supposed to be excited, say, from the left, by the fundamental eigenmode of a silicon slab waveguide with the same thickness. Complex amplitudes of slab eigenmodes transmitted to the right-hand side of the grating and reflected back are calculated (see Fig. 4a); the fractional power of these waves with respect to the input power is denoted as the

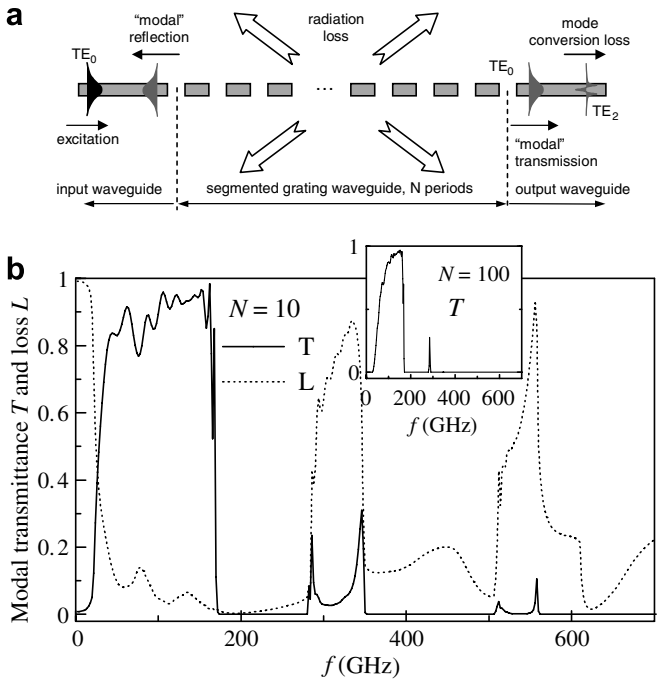

Fig. 4. Modal transmittance and loss calculated using the bi-directional mode expansion and propagation method. (a) Scheme of the principle of the method; (b) results of the calculation for 10 grating segments (main plot) and for 100 grating segments (inset; only the transmittance is shown).

modal transmittance T and reflectance R, respectively. All remaining fractional power is considered as the radiation loss L in the segmented region, $L = 1 - T - R$. Intrinsic absorption losses in silicon are neglected in this calculation.

The scheme of the principle of the method is shown in Fig. 4a. It makes use of the mode matching principle well-known in microwave engineering. Its first application for integrated optical waveguides was described in [30]. In [31], an efficient handling of periodic waveguide structures based on the application of Bloch modes was described. The results presented in this paper were obtained with its simple but numerically very stable version based on the expansion of the fields into a suitable set of orthogonal functions [32]. The results of this calculation are shown in Fig. 4b for $N = 10$ and 100 grating periods.

3. Discussion

The rigorous dispersion relation obtained using the modal method is plotted in Fig. 3. Only true guided modes can be found below the vacuum line: these modes do not exhibit any radiation losses as they cannot couple to other propagative modes in vacuum regions. In turn, these modes do not leave any fingerprints in the transmittance spectra.

All other modes plotted in Fig. 3 are leaky, with the exception of a few special values of $\omega(\beta)$. Note that their radiation losses are rather high: for comparison, the amplitude attenuation of THz radiation in lightly doped silicon ($\varepsilon = 11.68 + i0.008$) used in the experiment is only 0.074 cm^{-1} at 300 GHz (which corresponds to the imaginary part $0.65i$ GHz in the complex frequency representation used in Fig. 3).

Note that there is a set of modes with particularly high radiation losses for small longitudinal propagation constant β, which appear as wide oscillations in the transmittance spectra. For example, the radiation losses of the lowest mode above the vacuum line ($\omega = 275$ GHz for $\beta = 0$ cm^{-1}) reach 52 GHz. Such wide resonances are signatures of the Fabry–Pérot effect. For low frequencies, the grating behaves as a homogeneous slab with effective dielectric properties and the transmittance spectrum resembles that of a Fabry–Pérot resonator. Indeed, the frequency of the first broad maximum in the transmittance spectrum matches very well the frequency of this mode. The second mode of this type starts at 470 GHz. However, its relation to the Fabry–Pérot effect is less obvious as (i) the elevated frequency precludes the use of effective medium theories and (ii) the frequency of the broad transmittance maximum is affected by the presence of a sharp leaky mode in the same spectral range.

A remarkable feature in the dispersion relation is the existence of forbidden bands. The two lowest forbidden bands spread from 172 GHz to 269 GHz and from 353 GHz to 389 GHz, respectively. The electromagnetic radiation with frequencies belonging to the forbidden band cannot propagate inside the waveguide along the x-direction, and can only radiate into the free space. This fact is important e.g. for the design of efficient light-emitting diodes [33].

The results of the bi-directional mode propagation calculation are in a very good agreement with these conclusions: we compare here the spectra plotted in Fig. 4b with the dispersion curves shown in Fig. 3. The inset of Fig. 4b shows the two even true guided modes obtained for a simulation using a segmented waveguide with $N = 100$ periods. The first mode shows a cut-off frequency at 172 GHz and the second one is observed in the range 280–289 GHz: this is in a quantitative agreement with the dispersion curves shown in Fig. 3. The odd modes are not observed in this simulation because of the even symmetry of the TE_0 input mode (see Fig. 4a). (We note that a simulation with a TE_1 input mode – not shown here – yields a band at 275–300 GHz corresponding to the odd mode below the vacuum line in Fig. 3.) If the number of the segmented waveguide periods is decreased in the simulation to $N = 10$, leaky modes with small radiation losses start to be observed (see the main part of Fig. 4b). We point out again a very good agreement of these findings with the results of the modal approach: such modes occur close to the center and to the boundary of the first Brillouin zone, namely at 279, 340, 505 and 557 GHz. A small broad maximum in the modal losses near 450 GHz corresponds to the second even Fabry–Pérot mode of the structure.

It is also interesting to compare the rigorously calculated band structure with the band structure reconstructed from transmittance spectra. The agreement is very good for low

frequencies (for $\omega < \pi c/L$). In particular, the mode starting at 353 GHz at $\beta = 0$ cm^{-1} is clearly resolved in the transmittance spectra. The agreement is quite good also for the second and third even mode starting at 505 GHz and 610 GHz, respectively. However, the reconstruction of dispersion curves from the transmittance spectra becomes tricky for higher frequencies. Firstly, crossings of the dispersion curves of distinct leaky modes (e.g. in the spectral range around 450 GHz and 690 GHz) necessarily leads to a complicated shape of the transmittance spectra. Secondly, longer reciprocal lattice vectors start to play a role in Eq. (1), i.e., m becomes non-zero. This is equivalent to a mapping of the dispersion relation into the first Brillouin zone, which yields additional dispersion curves. Such a folding of dispersion curves is observed at the border of the first Brillouin zone at 565 GHz and also for several branches in the spectral range around 670 GHz. Although the rigorously defined band structure is unique, the dispersion curves obtained from the transmittance spectra do often considerably differ for different values of m.

4. Conclusion

Three methods were used for investigation of properties of a periodically modulated dielectric waveguide in the THz range. The rigorous modal approach allows us to identify the forbidden bands for the propagation along the waveguide. It also allows us to distinguish between (i) the true guided modes which propagate without radiation losses along the grating and which do not leave fingerprints in the transmission spectra and (ii) leaky modes which are guided along the structure but show radiation losses: these modes are detected in the transmission spectra.

The transfer matrix method yields the transmission spectra which are in a very good agreement with previously published experimental data and facilitates the connection of the experimental data to the band structure of the waveguide.

The approach based on the bi-directional mode expansion and propagation in the waveguide provides an independent check of the characteristics of true guided modes which are not accessible in the transmission experiments; it allows us also to identify the leaky modes characterized by small radiation losses.

For $f < 300$ GHz the grating behaves as a homogeneous slab with effective dielectric properties and the transmittance spectrum resembles to that of a Fabry–Pérot etalon (homogeneous waveguide). At higher frequencies leaky modes appear originating in resonant properties of segments: quantitative agreement between the experimental data and all three theoretical models remains very good. For $f > c/L$ the transmission spectra become very complex namely due to the contribution of longer reciprocal lattice vectors and the consequent folding of the dispersion relation to the first Brillouin zone.

Acknowledgements

Financial support by Academy of Sciences of the Czech Republic (Project No. 1ET300100401) and by Ministry of Education, Youths and Sports of the Czech Republic (Project OC 288.001) is acknowledged. One of us (J.-L.C.) would thank Prof. O. Parriaux for many stimulating discussions. Experimental data shown in this paper were achieved by E. Bonnet, M. Nazarov and G.-A. Racine.

References

[1] T. Mossberg, Ch. Greiner, D. Iazikov, Opt. Photonic News 15 (2004) 26.
[2] Z. Weissman, A. Hardy, J. Light-wave Tech. 11 (1993) 1831.
[3] E. Silberstein, P. Lalanne, J.-P. Hugonin, Q. Cao, J. Opt. Soc. Am. A 18 (2001) 2865.
[4] D. Eger, M. Oron, M. Katz, J. Appl. Phys. 74 (1993) 4298.
[5] E. Popov, M. Nevière, R. Reinisch, J.-L. Coutaz, J.-F. Roux, Appl. Opt. 34 (1995) 3398.
[6] M. Nevière, R. Petit, M. Cadihlac, Opt. Commun. 8 (1973) 113.
[7] S.T. Peng, T. Tamir, H.L. Bertoni, IEEE Trans. MTT 23 (1975) 123.
[8] Z. Weissman, A. Hardy, J. Lightwave Tech. 11 (1993) 1831.
[9] J. Čtyroký, J. Opt. Soc. Am. A 18 (2001) 435.
[10] D.D. Stancil, Appl. Opt. 35 (1996) 4767.
[11] S. Mishra, S. Satpathy, Phys. Rev. B 68 (2003) 045121.
[12] L. Li, J.J. Burke, Opt. Lett. 17 (1992) 1195.
[13] Q. Cao, P. Lalanne, J.-P. Hugonin, J. Opt. Soc. Am. A 19 (2002) 335.
[14] E. Bonnet, A. Cachard, A.V. Tishchenko, O. Parriaux, Proc. SPIE 5450 (2004) 217.
[15] E. Bonnet, A. Cachard, A.V. Tishchenko, O. Parriaux, F. Garet, J.-L. Coutaz, G.-A. Racine, Proc. SPIE 5466 (2004) 80.
[16] S.G. Johnson, P.R. Villeneuve, S. Fan, J.D. Joannopoulos, Phys. Rev. B 62 (2000) 8212.
[17] H. Benisty, D. Labilloy, C. Weisbuch, C.J.M. Smith, T.F. Krauss, D. Cassagne, A. Béraud, C. Jouanin, Appl. Phys. Lett. 76 (2000) 532.
[18] M.C. Nuss, J. Orenstein, Terahertz time-domain spectroscopy, in: G. Grüner (Ed.), Millimeter and Sub-millimeter Spectroscopy of Solids, Springer, Berlin, 1998, p. 7.
[19] J.-L. Coutaz, F. Garet, E. Bonnet, A.V. Tishchenko, O. Parriaux, M. Nazarov, Acta Phys. Pol. A 107 (2005) 26.
[20] E. Özbay, J. Opt. Soc. Am. B 13 (1996) 1945.
[21] M. Schuster, N. Klein, P. Ruther, A. Trautmann, O. Paul, P. Kužel, F. Kadlec, IEEE J. Sel. Areas Commun. 23 (2005) 1378.
[22] K. Sakoda, Optical Properties of Photonic Crystals, Springer-Verlag, Berlin, 2001.
[23] J.B. Pendry, A. MacKinnon, Phys. Rev. Lett. 69 (1992) 2772.
[24] S.M. Norton, T. Erdogan, G.M. Morris, J. Opt. Soc. Am. B 14 (1997) 629.
[25] R. Reinisch, J. Fick, P. Coupier, J.-L. Coutaz, G. Vitrant, Opt. Commun. 120 (1995) 121.
[26] J.B. Pendry, J. Mod. Opt. 41 (1994) 209.
[27] P.M. Bell, J.B. Pendry, L. Martín Moreno, A.J. Ward, Comput. Phys. Commun. 85 (1995) 306.
[28] M.C. Hutley, Diffraction Grating, Academic, London, 1982.
[29] R. Petit, Electromagnetic Theory of Gratings, Springer-Verlag, Berlin Heidelberg, 1980 (Chapter 5), p. 128.
[30] G. Sztefka, H.-P. Nolting, IEEE Phot. Technol. Lett. 5 (1993) 554.
[31] J. Čtyroký, S. Helfert, R. Pregla, Opt. Quantum Electron. 30 (1998) 343.
[32] J. Čtyroký, Opt. Quantum Electron. 38 (2006) 45.
[33] S. Fan, P.R. Villeneuve, J.D. Joannopoulos, E.F. Schubert, Proc. SPIE 3002 (1997) 67.